Tectonic and lithologic controls on the landscape adjustment along the eastern terrain of the Mae Tha fault, northern Thailand

Pichawut Manopkawee   Niti Mankhemthong   Chanin Pattarakamolsen

Department of Geological Sciences, Faculty of Science, Chiang Mai University
Chiang Mai, 50200, Thailand. Manopkawee E-mail: pichawut.m@cmu.ac.th

┤ A B S T R A C T ├

Understanding the interaction between tectonics, climatically-driven surficial processes, and bedrock erodibility provides insight into how the landscape develops over space and time. Although numerous active faults, lithologic and climatic variability control the landscape across Northern Thailand, the influence of these factors on the spatial adjustment of a dynamic landscape is largely unknown. In the study, we focus on lower-order channels developed across the eastern terrain of the Mae Tha fault, in which spatial variability in rock mass quality and fault characteristics strongly control the landscape. We combine topographic data analysis from channel profiles and geologic field observations to determine variations in bedrock watershed characteristics and any linear structures across the site. Our results reveal that channels in the northern and central zones of the terrain are relatively steeper because a west-dipping fault controls them with less fracture density of granite. Channels in the south, however, are less steep as an oblique-slip fault governs their profiles with a higher fracture density of bedrock. Moreover, channels flowing across different lithologic bedrocks exhibit steeper channel profiles than channels developed in uniform lithology. Our study highlights the use of topographic adjustment as one of the efficient tools to describe the dynamics of active deformation on the landscape over space and time. According to the mutual analysis, our finding suggests that lithologic resistance and spatial differences in fault lineaments ultimately control characters of channel profiles and overall landscape topography.

KEYWORDS │ Mae Tha fault. Landscape adjustment. Longitudinal channel profiles. Channel steepness. Rock uplift.

INTRODUCTION

Landforms in tectonically active settings are the product of an interaction between tectonics, climatically-driven fluvial erosion, and bedrock resistance (Dietrich *et al.*, 2003; Whipple, 2009; Whittaker *et al.*, 2008). Such an interaction governs topography and topographic relief as tectonics acts to change regional surface elevations via differential rock uplift, climate modulates erosional processes and sediment transport along topographic gradients, and bedrock properties play a central role in governing rates and patterns of landscape responses to denudational processes (DiBiase *et al.*, 2015; Schmidt and Montgomery, 1995). Understanding these factors that control spatial changes on erosional landscapes remains a first-order challenge in geomorphology and tectonics.

To measure the deformation due to tectonic processes, an exposure of a piercing point or a linear/planar geomorphic marker allows the magnitude of displacement to be determined. At fluvial systems in a faulted terrain, we may observe geomorphic markers such as an offset stream

on an alluvial fan or traces of active faults. The difference between pre-deformational geometry and the presently offset features can inform about tectonic and climatic shifts and the degree of deformation (Burbank and Anderson, 2012). However, the preservation of geomorphic features is poor when they are old and/or exposed to extreme climatic conditions. Due to the scarcity of fluvial terraces allowing to mark episodic tectonic uplift, several studies have focused on a theoretical framework that channel networks in active regions can demonstrate the relationship among adjustment of longitudinal channel profiles, surface elevation, and topographic relief (Howard *et al.*, 1994; Tucker, 2004; Whipple and Tucker, 1999): channels define local relief structure of the landscape (Hilley *et al.*, 2019), transmit signals of changes throughout a landscape via the progressive upstream migration of knickpoint (Kirby and Whipple, 2012; Whipple and Tucker, 1999; Wobus *et al.*, 2006), and redefine a lower boundary condition for adjacent hillslopes. The responses of hillslopes always lag behind channel incision along channel networks (Hurst *et al.*, 2012). In a steady-state landscape, the variations in longitudinal channel profiles suggest a spatial landscape adjustment and help to infer rock uplift over space and time conditions (Kirby *et al.*, 2003, 2007; Kirby and Whipple, 2001). Using longitudinal profiles of bedrock channels to describe active deformation on the landscape has been successful in several active mountain belts worldwide (Kirby *et al.*, 2003, 2007; Kirby and Whipple, 2001).

Since the bedrock channel incision model has been developed (Howard *et al.*, 1994; Snyder *et al.*, 2003; Whipple and Tucker, 1999), we hypothesize that the longitudinal profiles of bedrock channels potentially encode information on the base-level lowering, rock uplift, and channel incision (Duvall *et al.*, 2004; Kirby *et al.*, 2003). As rock uplift rates increase, channels steepen, and the steepness becomes a more effective agent of channel erosion. The findings illustrate that channel steepness positively correlates to rock uplift rates (Wobus *et al.*, 2006). Recent studies suggest that rock uplift firmly controls channel steepness and presumably dictates landscape adjustment in tectonically active settings (Hurst *et al.*, 2019; Kirby *et al.*, 2003, 2007).

Although tectonic processes and lithology worldwide have been extensively mapped, we still need insight into how tectonics and lithology govern landscape changes over space and time. A single discovery does not apply everywhere on the Earth. An understanding of the factors that control various geological sites can provide more information about the dynamic deformation of landscapes. In this research paper, we aim to directly extract signals of active deformation on a landscape from channel longitudinal profiles at a site where tectonic evolution and lithology are known a priori. We evaluate variations in channel morphology and assess the manner in which tectonic and lithologic factors control the adjustment of bedrock channels and landscape topography.

Overview of bedrock incision model

In most bedrock channels in tectonically active regions, the detachment-limited bedrock channel erosion rate, E, is a power-law function of contributing drainage area, A, (a proxy for local channel discharge) and channel gradient, S (Howard *et al.*, 1994; Stock and Montgomery, 1999; Tucker, 2004). The equation can be written as:

$$E = KA^m S^n \qquad (1)$$

where K is the erodibility coefficient incorporated substrate-, climate-, geometric-, and hydrologic-dependent variables, and m and n are exponents related to geometry, basin hydrology, and incision processes (Howard *et al.*, 1994; Tucker, 2004; Whipple *et al.*, 2000). The evolution of channel longitudinal profiles states that the change in channel bed elevation ($\frac{dz}{dx}$) at any point along the profile reflects a competition between rock uplift, U, and channel erosion rate, E, relative to a fixed base level as:

$$\frac{dz}{dx} = U_{(x,t)} - E, \qquad (2)$$

$$\frac{dz}{dx} = U_{(x,t)} - KA^m S^n \qquad (3)$$

where x is the location and t is the time. Under a steady-state condition ($\frac{dz}{dx} = 0$), channel erosion equals to rock uplift rate. The steady-state channel gradient, Ss, is expressed as:

$$S_S = \left(\frac{U}{K}\right)^{1/n} A^{-m/n} \qquad (4)$$

The empirical form of equation (4) is often observed in a wide variety of natural landscapes. Equation (4) can be rewritten as:

$$S_S = k_s A^{-\theta} \qquad (5)$$

where K_s describes the steepness of the channel profile, and θ is the rate of change of local channel gradient relative to an increasing drainage area (Flint, 1974; Wobus *et al.*, 2006). K_s and θ are channel steepness and channel concavity indices, respectively. The channel steepness index, K_s, as a function of the rate of rock uplift, U, and erosional coefficient of the substrate, K, can be described as:

$$k_s = \left(\frac{U}{K}\right)^{1/n} \qquad (6)$$

$$\theta = \frac{m}{n} \qquad\qquad (7)$$

According to equation (6), channel steepness, K_s, is affected by U, K and n. The rock uplift rate U, depends on the change of channel bed elevation through time, whereas the erosional coefficient, K, amalgamates factors of lithology, climate, and sediment load (DiBiase and Whipple, 2011; Lague *et al.*, 2005; Snyder *et al.*, 2003; Tucker, 2004). The slope exponent, n, is assigned to the value of 2/3 or between 0.35-0.6 (Stock and Montgomery, 1999; Whipple *et al.*, 2000).

Bedrock incision model describes that the erosional efficiency can increase when the lithologic substrate is more erodible, precipitation is promoted, and sediment load is more available in channel networks. It is noted that increasing erosional efficiency may increase channel networks to steepen watersheds, narrow channel widths, and a high potential for channel erosion (Yanites and Tucker, 2010). Thus, our study uses the simple bedrock incision model to explain the response of channel morphology and landscape topography to variations in lithologic and tectonic forcing where climatic conditions are relatively uniform.

Study site: Mae Tha fault in Chiang Mai and Lamphun provinces

The study site is located along the eastern side of Chiang Mai (CM) and Lamphun (LP), Thailand, where three main watersheds: Mae Ngat and Mae Khot rivers, Mae Kuang and Mae On rivers, and Mae Tha river, feed to Chiang Mai Basin in the west (Fig. 1A). The direction of rivers in these watersheds follows the different orientations of the Mae Tha Fault Zone (MTFZ) which illustrate as "S" shape /or semicircular structure with the total length of over 100km.

The MTFZ, composed of 52 fault segments, cuts through several rock types. Along the eastern side of the MTFZ, high terrain in the northern zone is intruded by Triassic Khun Tan-Doi Saket-Wiang Pa Pao granitic and granodioritic batholiths that mainly composes of quartz and alkali-and calcium-rich feldspar (Charusiri *et al.*, 1993). The lower parts of the terrain are mantled by Carboniferous massive sandstone interbedded with siltstone and shale of the Mae Tha group and Silurian-Devonian low-to-medium grade metamorphic rocks. The western block of the MTFZ is underlain by Paleozoic clastic rocks to Quaternary unconsolidated materials (Fig. 1B) (Mankhemthong *et al.*, 2020). The climatic condition across this region is a tropical climate. Precipitation is from southwest monsoon between June and October, while the rest of the year is hot summer and cool winter. The mean annual accumulated rainfall ranges between 1100 and 1300mmyr[1] over the period

1981-2010 (Fig. 1C). Regarding the unique watershed with different orientations of faults in the MTF, the terrain is classified into three main sections:

• The northern section, which is bounded to the east by the normal fault, is in Mae Ngat and Mae Khot rivers watershed.
• The central section, which lies along the oblique-slip fault within Mae Kuang and Mae On river watershed.
• The narrow southern section within the Mae Tha river watershed.

Due to occurrence of numerous small fault segments in the MTFZ, some small fault segments named by Wiwegwin *et al.* (2018) and Department of Mineral Resources (2020) are significant regarding seismicity, geomorphic features, and landform evolution. We group the following segments: Doi Chom Hot (DCH), Nam Mae Pang (NMP), Doi Pui (DP), Huai Pang Sanuk (HPS), Nam Mae Lai (NML), Huai Ta Dam (HTD), Doi Nam Khun (DNK), Doi Huai Luek (DHL), Huai Sai Khao (HSK), Haui Mae Sa Puat (HMS), and Doi Mae Tueng (DMT) into a single fault called "Mae Tha fault"/or the MTF (Fig. 2A). Our study mainly focuses on the eastern block of the MTF.

An elevation profile was obtained to get topographic information across the eastern block of the MTF (Fig. 2B). The topographically rugged terrain has a relatively constant elevation in the northern and central sections. The maximum elevation is approximately 1900m at Doi Phi Pan Nam (PPN) and Doi Mae Tho (DMT) in the central section of the study site (Fig. 2A-B). The surface elevation decreases to Kew Fin (KF) and Doi Khun Tan (DKT) toward the south with the smaller intermontane basin in Mae Tha district, Lamphun. The decreases in elevation and topographic relief are not apparent from variable lithologic materials. Based on a transverse hypsometric integral (THI) and the approach proposed by Pérez-Peña *et al.* (2009), moreover, landform evolution is between the youthful stage and the mature stage because the rugged terrain is typically bounded by deep and steep-sided valleys (Fig. 2C).

The MTF is considered a moderate-to-high active fault zone due to recently numerous small (magnitude, Mw< 5) to moderate (Mw 5-7) earthquakes across Northern Thailand (Department of Mineral Resources, 2020; Pailoplee and Charusiri, 2016). According to the study of Optically Stimulated Luminescence (OSL) and Carbon-14 age of sediment samples in trench sites where the MTF passes through (Fig. 3), the study reveals at least four times paleo-earthquake occurrences at the age of 25,000, 24,000, 5,000, and 1,500 years ago. The slip rate of the MTF is estimated as 0.1-1mmyr[1]. The recurrence interval of large earthquakes is predicted at 1,000 years (Department of Mineral Resources, 2008, 2018). Furthermore, geomorphic

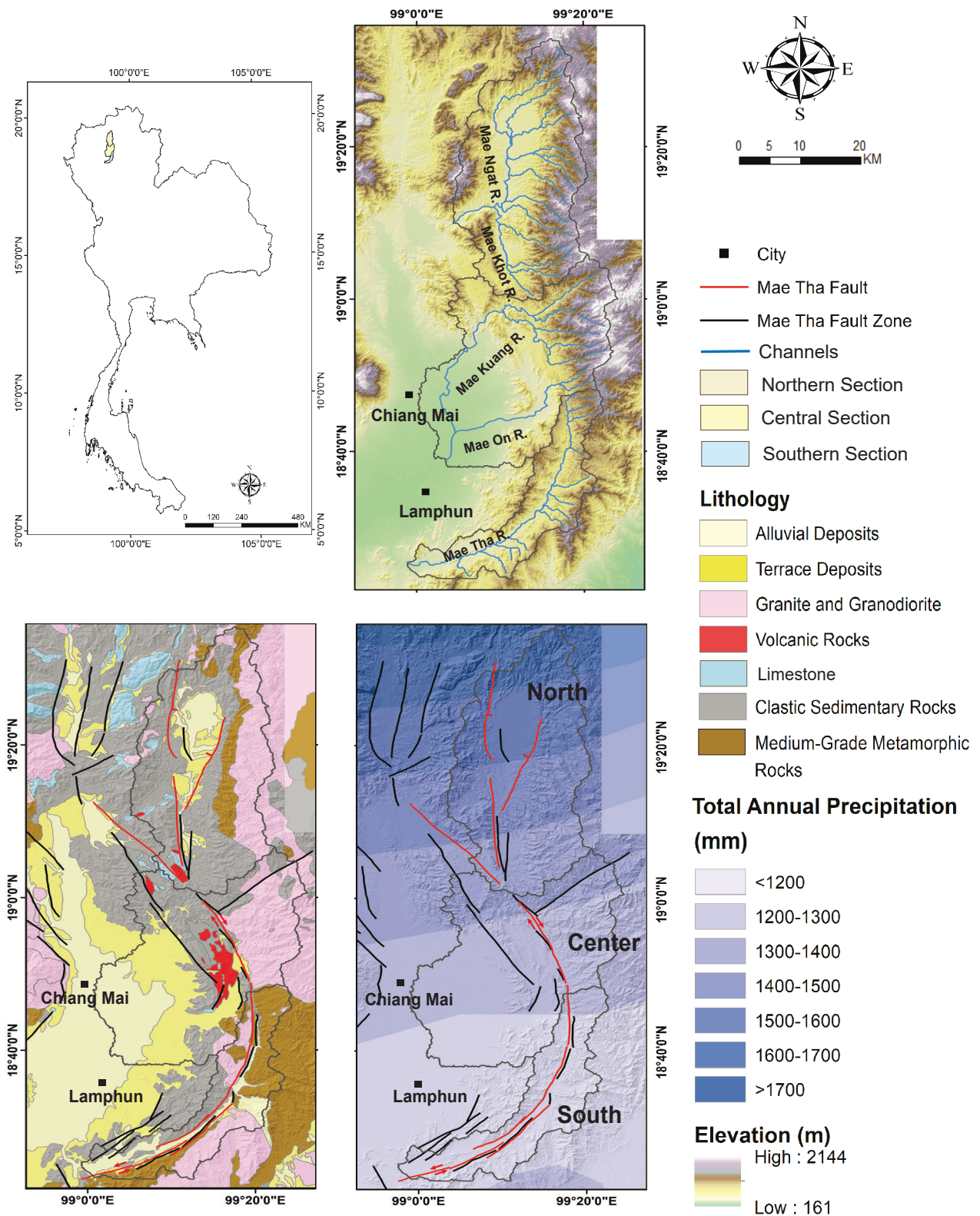**FIGURE 1.** Geomorphic settings of the study site. A) Map of Thailand with the location of the study area. B) Location of the study site with three main watersheds; North: Mae Ngat and Mae Khot rivers, Center: Mae Kuang and Mae On rivers, South: Mae Tha river. These rivers feed Chiang Mai and Lamphun in the west. C) Geologic setting of the study site (Modified from Mankhemthong *et al.*, 2020). North segments of the fault are defined as normal faults, while the Central and South segments of the fault are strike-slip faults. D) Map of the distribution of 30-year period accumulated rainfall during 1981-2010. Although accumulated rainfall varies from north to south, the assumption of the minimal variation in rainfall has been made in the study (Modified from Khamkong *et al.*, 2017). The geomorphic settings of the study site are categorized into three sections: North, Center and South.
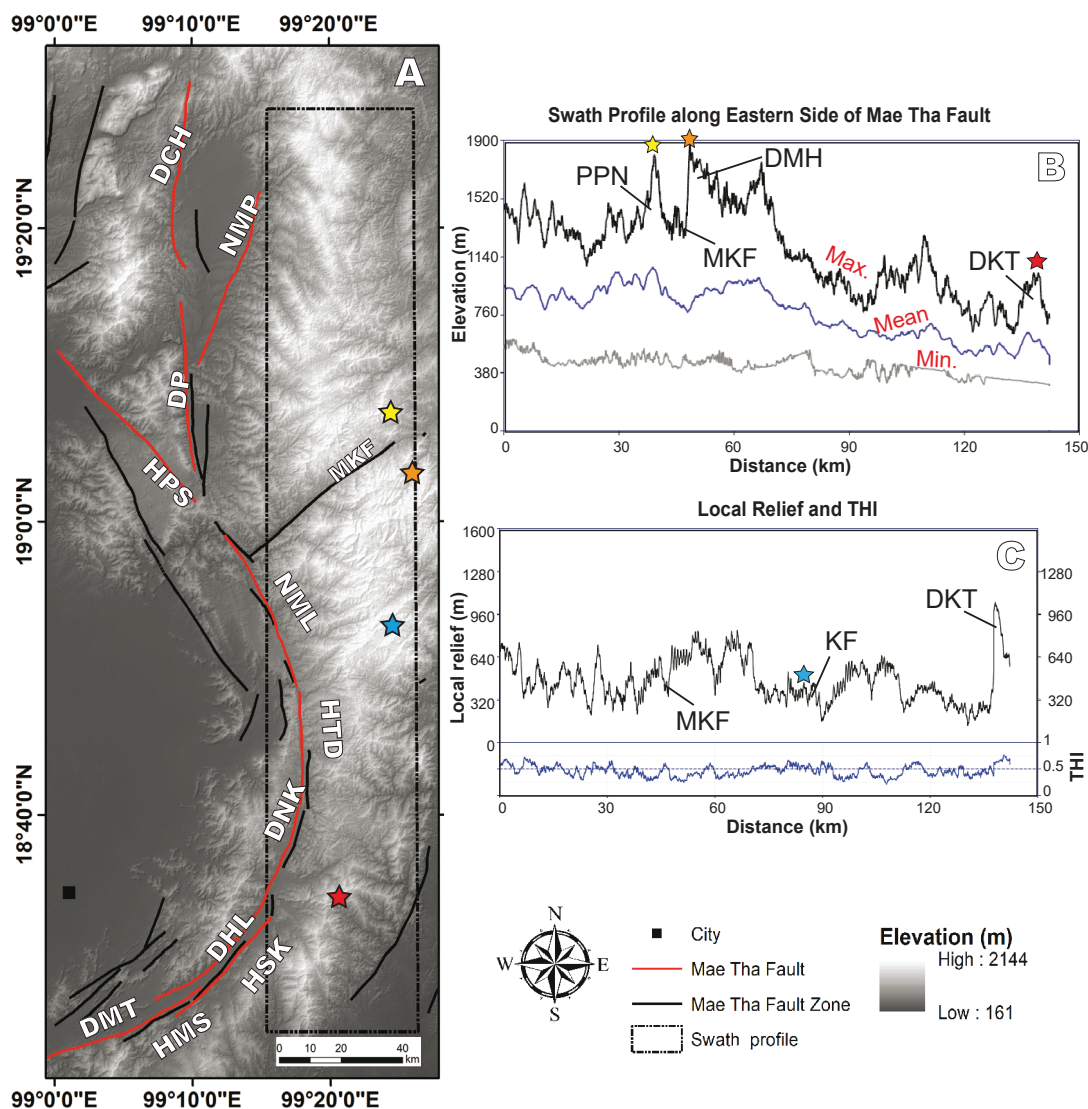
FIGURE 2. Topographic and physiographic features of the MFTZ. A) The MTF (red line) includes a series of faults as follows: DCH: Doi Chom Hot; NMP: Nam Mae Pang; DP: Doi Pui; HPS: Huai Pang Sanuk; NML: Nam Mae Lai; HTD: Huai Ta Dam; DNK: Doi Nam Khun; DHL: Doi Huai Luek; HSK: Haui Sai Khao; HMS: Huai Mae Sa Puat and DMT: Doi Mae Tueng (Wiwegwin *et al.*, 2018; Department of Mineral Resources, 2020). B) The swath topography profile along the rectangle marked in Figure 1B-D represents the relatively constant elevation in the northern and central zones and the decrease in elevation toward the south. Maximum, mean and minimum elevation extracted from a 15km wide swath profile (Fig. 2A). C) High topographic relief across the study site corresponds to the variation in elevation profile (Fig. 2B). Transverse Hypsometric Integral (THI) is approximately 0.5, implying that the age of the landscape evolution is between the youthful stage to maturity. Abbreviations and symbols in Figure 2A-C are PPN: Doi Phi Pan Nam (yellow star); DMH: Doi Mae Tho (orange star); MKF: Mae Kuang Fault, DKT: Doi Khun Tan (red star); KF: Kew Fin (blue star).

features in each section of the study site are preserved on the resistant bedrock along the MTF, such as triangular facets, wineglass canyon, offset streams, and shutter ridges, and are shown in Figures 3-5.

The development of channels and landscape topography across the eastern side of the MTF reflects a dominant tectonic and litho-structural control, apparently little influenced by the variation in mean annual accumulated rainfall of the area compared to regional climatic gradients across Northern Thailand.

METHODS

Analysis of geomorphic indices on channels

To investigate the spatial variation in channel morphology on the eastern block of the MTF, we targeted 35 first-order watersheds draining to the west to collect a series of longitudinal channel profiles (the height of the channel bed along the entire course of the channel), contributing drainage areas, and channel gradients. These data are used to calculate variations in geomorphic indices
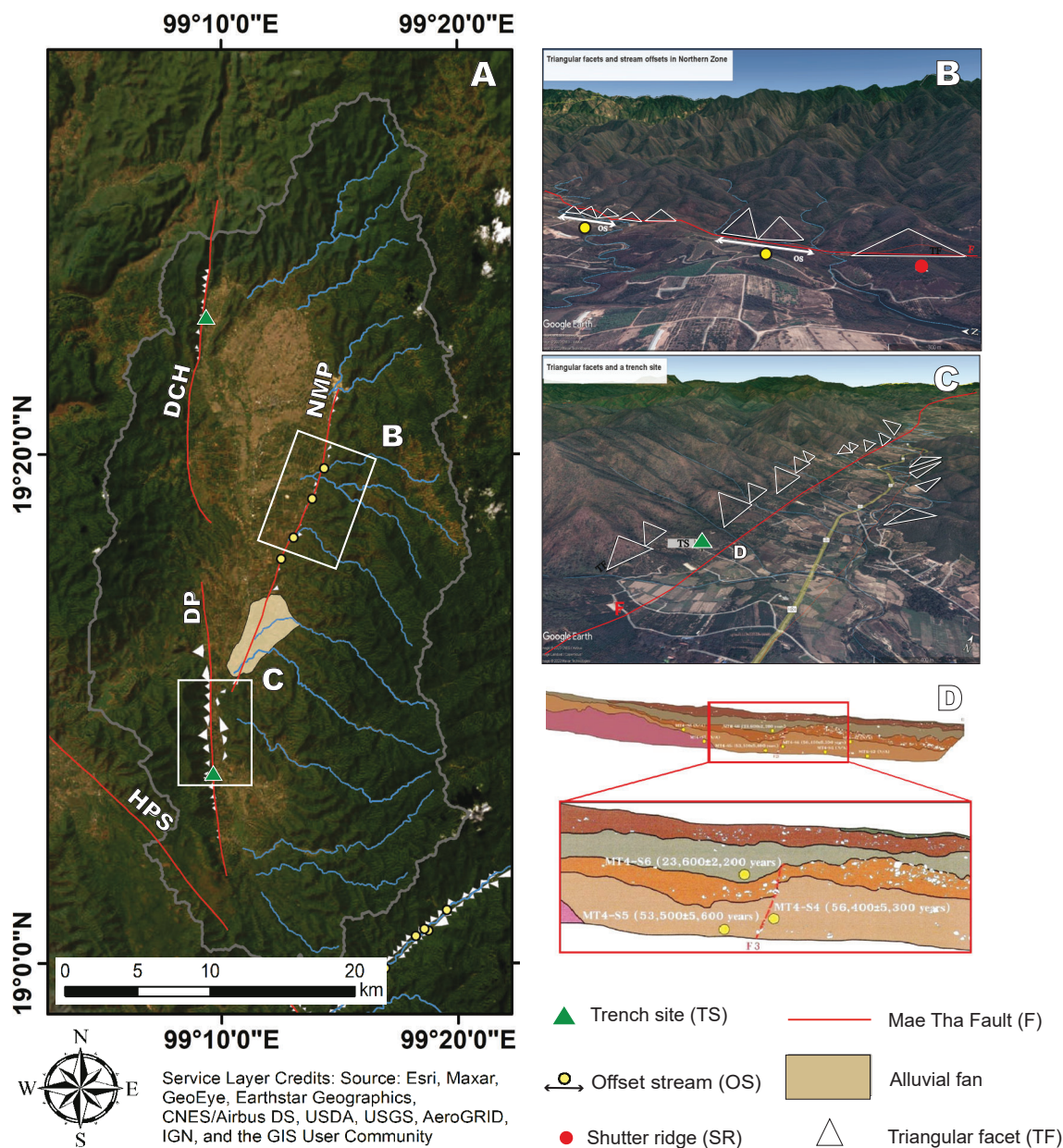
FIGURE 3. Geomorphic features of the study site. A) The fault segments of Doi Chom Hot (DCH), Nam Mae Pang (NMP), Doi Pui (DP) and Huai Pang Sanuk (HPS) show in the northern section derived from Google Earth Pro®. White rectangles represent examples of geomorphic features shown in Figure 3B-C. B) Triangular facets, offset streams, and shutter ridges along the Nam Mae Pang fault segment. C) Triangular facets and trench sites along the Doi Pui fault segment. D) The north wall of Ban Long Khot trench site, Phrao district, Chiang Mai, illustrates that the fault cuts through bedrock (pink color) and overlying stratified sediment on alluvial terraces (pale and dark orange color). Doi Pui fault segment is a normal fault with 0.1mmyr⁻¹ slip rate, 13,000 years recurrence interval and 24,000 years elapsed time (Department of Mineral Resources, 2008).

(channel steepness and channel concavity indices) from north to south.

Extraction of longitudinal channel profiles

We exploited the 12.5 meter Digital Elevation Model (DEM) collected and produced by Synthetic Aperture Radar from the ALOS satellite, Alaska Satellite Facility (ASF) (Laurencelle, *et al.*, 2015). The DEM has proceeded through Radiometric Terrain Corrected (RTC) to correct the backscatter intensity of pixels and improve the resolution. We extracted 35 lower-order watersheds along the eastern terrain of the MTF. These 35 watersheds have relatively similar channel lengths (~9km) with averaged contributing drainage areas of 138km². The effects of
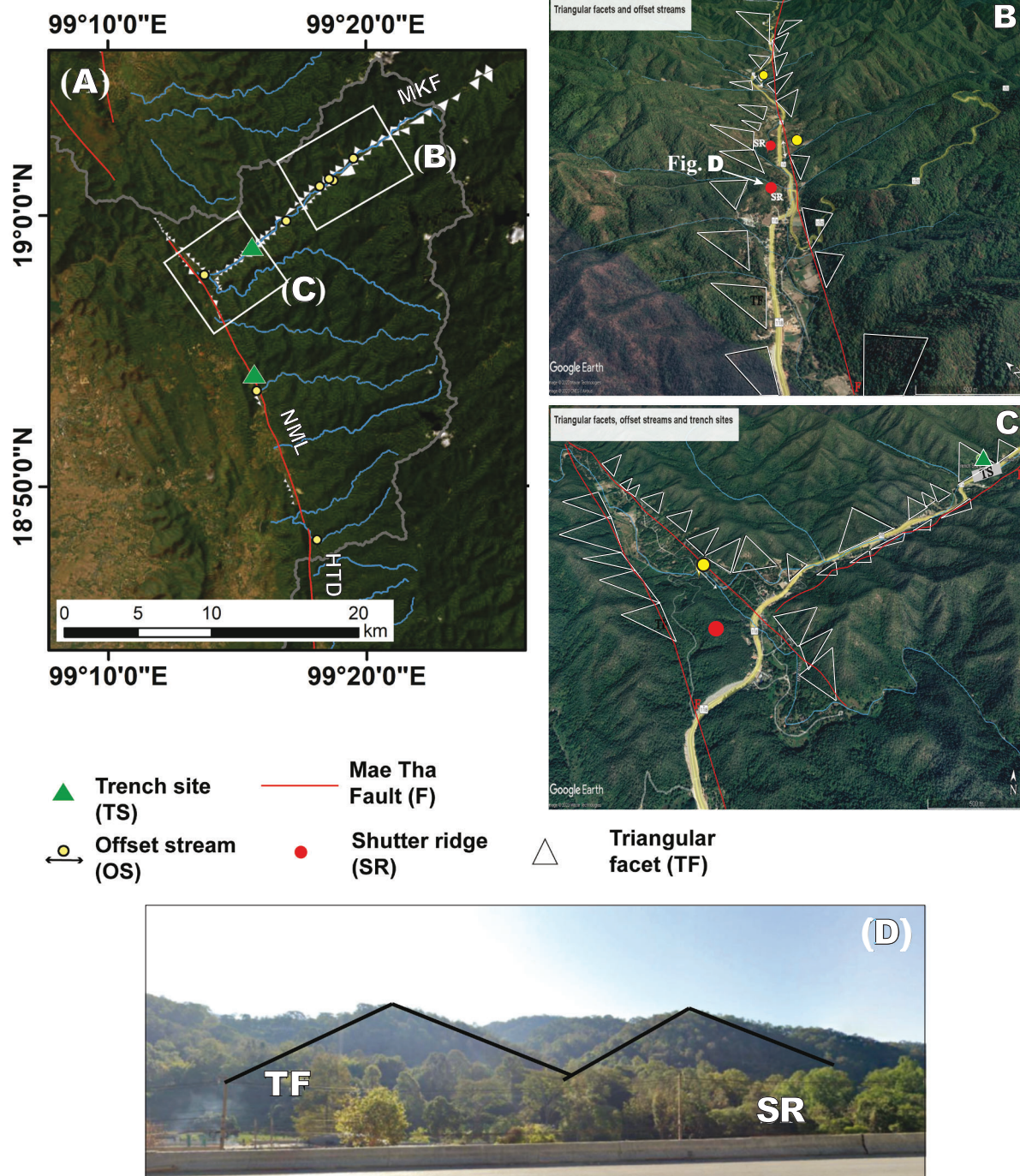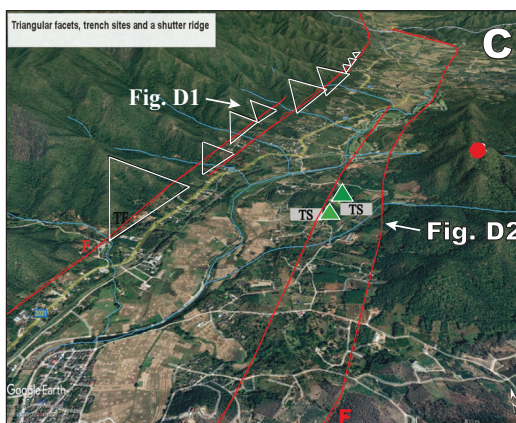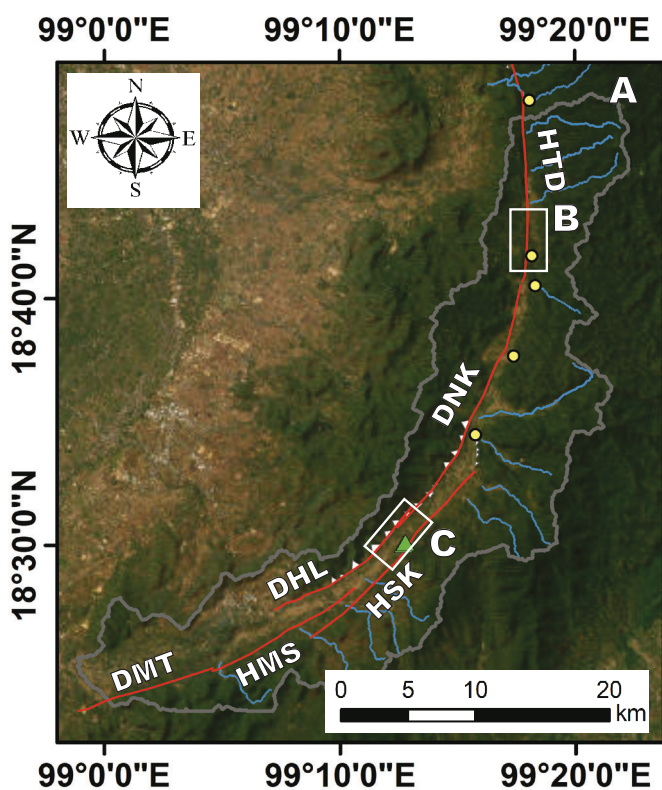
FIGURE 4. Geomorphic features of the study site. A) The fault segments of Nam Mae Lai (NML), Mae Kuang (MKF) and Huai Ta Dam (HTD) show in the central section derived from Google Earth Pro®. White rectangles represent examples of geomorphic features shown in Figure 4B-C. B) Triangular facets, offset streams, and shutter ridges along Mae Kuang fault. C) Triangular facets, an offset stream, shutter ridges, and Pong Aor trench sites along Mae Kuang fault. D) Triangular facets along the Thai National Highway 108 with a shutter ridge in the front.

variable watershed sizes were minimized. Longitudinal channel profiles were also extracted for the channels in the southern section, even though they were of shorter length and smaller drainage size than those in the northern and central sections.

To begin with channel profile extraction, we implemented a continuous method to extract topographic parameters while recording elevation, cumulative downstream distance, and contributing drainage areas. We used built-in scripts of
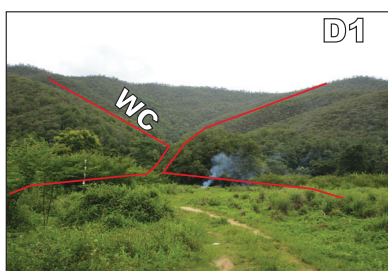
FIGURE 5. Geomorphic features of the study site. A) The fault segments of Huai Ta Dam (HTD), Doi Nam Khun (DNK), Doi Huai Luek (DHL), Haui Sai Khao (HSK), Huai Mae Sa Puat (HMS) and Doi Mae Tueng (DMT) show in the southern section derived from Google Earth Pro®. White rectangles represent examples of geomorphic features shown in Figure 5B-C. B) Shutter ridges and an offset stream along the Huai Ta Dam fault segment. C) Triangular facets, shutter ridges and Tha Pla Duk trench sites along the Haui Sai Khao fault segment. D) Drone survey images show a wineglass canyon along Doi Huai Luek fault segment (D1), large triangular facets and a fault trace along the Haui Sai Khao fault segment (D2).

the hydrologic toolset in ArcGIS to create hydrologic related-flows and delineate drainage basin areas. We also used a suite of MATLAB scripts of the Stream Profiler tool, developed by Snyder *et al.* (2000) and Whipple *et al.* (2007), to extract and analyze the longitudinal channel profiles. We filtered the elevation data by passing a moving average window of 25 pixels across the DEM. The moving window method allows for minimizing noise associated with the raw data of the

DEM while maintaining longitudinal channel profiles. We set the constant vertical interval at 5m from the smoothed elevation data to calculate local channel gradients.

Analysis of longitudinal channel profile

In the Stream Profiler tool, we turned channel profiles into a plot of an empirical scaling relationship between

channel gradients (S) and upstream drainage area (A). Such the relationship is cast similar to equation (5) in terms of channel steepness (K_s) and concavity index (θ). We regressed a log-log plot of local channel gradients against upstream drainage areas, following the approach of Wobus *et al.* (2006). The regression line partially captures a detachment-limited bedrock fluvial channel section, and the line excludes debris-flow-dominated reaches at headwater and depositional sections at downstream reaches. The break in the channel profile is known as an abrupt change in channel gradients with increasing upstream drainage areas (Snyder *et al.*, 2000; Stock and Dietrich, 2003; Wobus *et al.*, 2006). The regression line independently fits on the sub-section of channels if the abrupt change in channel gradients appears.

To spatially compare channel steepness among different channel segments of varying upstream drainage areas and concavity index, a suite of normalized channel steepness indices (k_{sn}) is generated with a fixed reference concavity index at 0.45 (θ_{ref}= 0.45) (Wobus *et al.*, 2006). Normalized channel steepness indices could be calculated as

$$k_{Sn} = S_s A^{\theta ref} \qquad (8)$$

The difference in k_{sn} does not depend on θ_{ref}. It effectively compares k_{sn} for channels with different upstream drainage areas (Duvall *et al.*, 2004; Howard *et al.*, 1994; Kirby and Whipple, 2012; Snyder *et al.*, 2003).

Analysis of lineaments: faults and fractures

The MTF generates moderate-to-high seismic activities. Rock failures and deformation result from seismic events and igneous intrusion into local rocks. The permeable fracture zones in the rocks allow hydrothermal fluid to flow from the depth to the shallower level. To investigate the level of rock strength across the active region, we determined the fracture density -an evaluation of lineament density generated by the connection between faults and fractures. We used aerial and satellite images provided by Google Earth Pro® and high-resolution DEM to identify all lineaments and infer the impact of different levels of tectonic forcing across the landscape.

Characterization of structures and fracture density

Although the zone of rock failures related to the MTF is broad, we could not observe smaller lineaments on digital images and DEM because forest is densely populated. The detail on fractures and fracture density is still unknown. Because of the recent advances in high-resolution digital topographic data providing a more accurate description of landscape features, fractures in the landscape can be determined by the finer routes of channels on the landscape using a suite of hydrologic-related flows in ArcGIS. Once

we calculated flow direction and flow accumulation on the DEM, the threshold of flow pixels was reduced to 500 accumulated flow pixels to magnify the possible channel flow paths. We inferred the occurrence of fractures on the landscape from the theory that rectangular drainage patterns or the channels with right-angle bends reflect the rectangular patterns of bedding planes, faults, and fractures (Howard, 1967; Mejia and Niemann, 2008).

To compare the spatial distribution of fractures across the region, we assigned weights to different magnitudes of each lineament: the MTF was assigned a weight of 3, minor faults were given a weight of 2, inferred fractures were assigned a weight of 1, and a weight of 0 was given to other areas that are not associated with any lineaments (Table 1). We calculated the fracture density as the ratio of the summation of the weight values for each rank and the length of each rank within a constant circular search radius of 3km (Liu *et al.*, 2012). It was calculated as

$$D = \frac{(\sum wL)}{A_{SR}} \qquad (9)$$

where D is fracture density, w is the weight of each rank, L represents the lineament length of features, and A_{SR} is the constant area of the search radius.

Conventional and drone geological field surveys

We conducted an extensive geological field survey to investigate evidence of fault traces and other lineaments on the landscape at both landscape-and local-(outcrop) scales and to measure sediment bedload at the location of the intersection of the MTF and channels. We started surveying roadcut outcrops along the Thai National Highways 1150, 1001 in Phrao district, Highway 118 in Doi Saket district, and Highway 1230 in Mae On and Mae Tha districts to explore any rock surfaces that potentially preserved evidence of polished surface (slickensides) and a series of parallel lines (slicken lines). We observed the preserved structures on rock surfaces at sites where the trace of MTF is present (Fig. 6A-E). These kinds of evidence could indicate the paleo-kinematics of the fault. Moreover, we surveyed lineaments

TABLE 1. Weights of lineaments

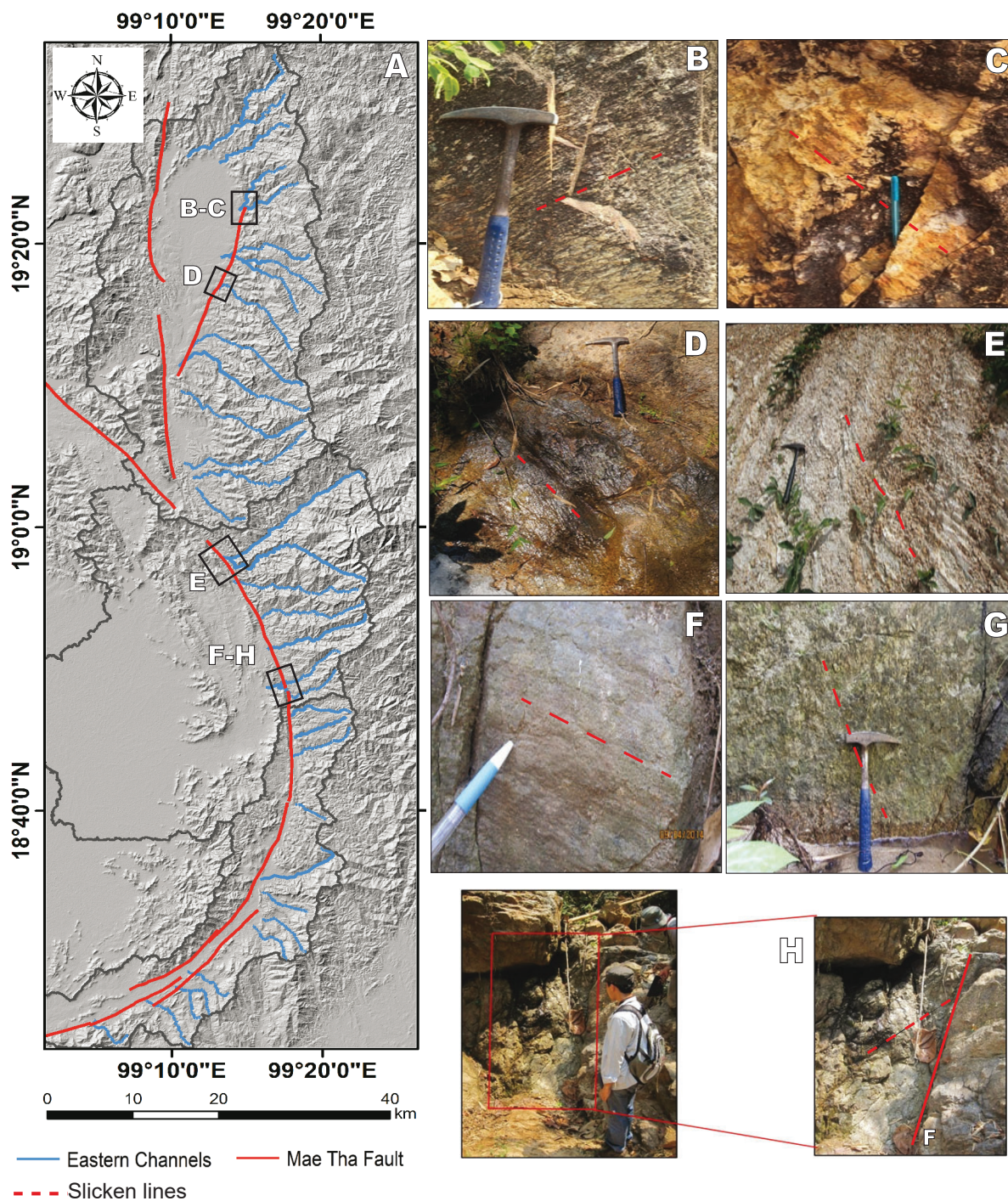| Lineament magnitude	Weights (w)
Major Structure (MTF)	3
Minor Structures	2
Inferred Fractures	1
None	0

FIGURE 6. Field observations of landscape topography along the MTF. A) Map of the study site with 35 channel locations. Black rectangles indicate field locations where evidence of lineaments has been observed on the landscape. B) Slicken lines (small red dashed lines) orient at 50º/355º on a fault plane at 003º/72ºNW. C) Slicken lines orient at 49º/244º on a fault plane at 226º/81ºNW. D) Slicken lines orient at 36º/113º on a fault plane at 074º/41ºSE. E) Road-cut outcrop along the Thai National Highway 118. F-G) Examples of slicken lines are shown on exposed granitic rocks along Mae On and Mae Ruam rivers. Slicken lines are measured and shown in Figure 11. H) Exposed fractured granite with a scale of 170cm along Mae On and Mae Ruam rivers. A red line shows a minor fault line.

along Mae On and Mae Ruam rivers, where these rivers flow perpendicular to the MTF (Fig. 6F-H). The appearance of slickensides and slicken lines preserved on granitic rock surfaces was exposed throughout the length of the rivers.

We did not observe slickensides and slicken lines on rock surfaces in the southern section. Thus, we operated a drone to survey some fault-related geomorphologic features and evidence of lineaments at a landscape scale, for example,

fault scarps, triangu (lar facets, wineglass canyons, offset channels, and alluvial fans. The drone was limited to fly at a maximum height of 90m above the ground.

Characterization of sediment particles

We surveyed eight channels from north to south to generate an extensive dataset of their grain size distribution (Fig. 7). For each channel, we started at the intersection of the trace of the MTF and channel route and surveyed approximately 100m upstream. The selection of channels was planned to survey channels with a wide range of channel steepness indices.

We used the Wolman pebble count procedure to characterize sediment grain size distribution as we measured the sizes of random particles using the United States Geological Survey (USGS) gravelometer (Fig. 7B-C). We randomly collected a minimum of 100 sediment particles using a zigzag pattern across the surveyed channels 5, 7, 11, 17, 19, 22, 25, and 30 (Fig. 7D-I). The collection of sediment grain size was calculated and classified as the range of a fraction of different particle sizes (*e.g.* D_{10}, D_{50} and D_{90}). To efficiently compare variations in sediment particles, we assumed that downstream fining and grain size reduction was minimal in lower-order channels. The nature of the collected sediments reflects the lithologies of the whole drainage area.

RESULTS

Spatial variations in channel steepness indices

The analysis of longitudinal channel profiles reveals the spatial variations in channel gradients and channel steepness indices along the eastern terrain of the MTF. Less than half of all channels exhibit smooth, concave-up profiles that represent steady-state conditions (Fig. 8A). However, more than half of all channels in the northern and central parts of the landscape are in a transient-state condition because they represent convex knickpoints that separate steeper upper portions from gentler lower reaches (Fig. 8B). Examples from Figure 8 show longitudinal channel profiles extracted along the eastern side of the MTF and are further described below.

The normalized channel steepness indices (k_{sn}) represent a decrease from north to south (Fig. 9A-B). Taking a reference concavity index of $\theta_{ref}= 0.45$, channels in the northern zone exhibit the highest $k_{sn}\sim140m^{0.9}$ at channel 4 and reflect high channel and hillslope gradients. k_{sn} values decrease toward 60-80$m^{0.9}$ in the central zone and reach a minimum value of ~20$m^{0.9}$ at channel 35 in the south (Fig. 9B). Table 2 represents the variation in topographic

TABLE 2. Topographic characteristic of channel profiles along the eastern side of the MTF*. [a]Channel number starts from the northern tip of the segment (Fig. 9A). [b]Read 3.70E+07 as 3.7 x10^{7}. [c]Calculated with $\theta_{ref}= 0.45$. *Italics depict channel steepness indices of channel reaches above knickpoint

| Channel[a]	A_{min} (m²)[b]	A_{max} (m²)	θ	k_s	k_{sn} (m^0.9)[c]
1	3.70E+07	1.73E+08	2.56	1.62E+18	37.36
	1.02E+06	*4.03E+07*	*0.64*	*2.33E+03*	*80.54*
2	8.92E+06	8.73E+07	0.82	3.90E+04	54.65
	9.82E+05	*8.81E+06*	*0.11*	*5.55E-01*	*71.32*
3	7.60E+06	4.97E+07	1.45	1.50E+09	51.54
	3.80E+05	*7.76E+06*	*0.04*	*3.22E-01*	*82.97*
4	1.01E+07	3.05E+07	1.71	6.87E+10	61.13
	8.47E+05	*4.53E+06*	*0.90*	*9.57E+04*	*138.54*
5	1.80E+07	8.76E+07	2.29	4.75E+15	58.77
	1.94E+06	*5.70E+06*	*1.45*	*5.77E+08*	*123.09*
6	1.16E+07	2.48E+07	2.37	5.62E+15	67.78
	8.86E+05	*3.52E+06*	*1.32*	*3.24E+07*	*136.25*
7	3.70E+07	1.04E+08	2.95	1.50E+21	33.34
	1.80E+07	*5.01E+07*	*2.11*	*2.26E+14*	*121.55*
	9.14E+05	*1.74E+07*	*0.64*	*1.04E+03*	*40.44*
8	2.48E+07	9.36E+07	2.18	1.49E+15	46.74
	3.87E+06	*2.66E+07*	*0.84*	*5.23E+04*	*76.66*
9	1.56E+07	3.12E+07	1.85	1.79E+12	63.29
	1.77E+06	*1.36E+07*	*0.45*	*1.16E+02*	*97.38*
10	2.48E+07	5.41E+07	1.69	1.03E+11	43.01
	8.61E+06	*2.42E+07*	*-0.46*	*4.42E-05*	*115.06*
	2.75E+05	*5.08E+06*	*0.42*	*2.08E+01*	*26.93*
11	2.38E+07	4.78E+07	2.98	8.31E+20	59.72
	8.95E+04	*2.70E+07*	*0.46*	*8.08E+01*	*64.27*
12	1.24E+07	4.12E+07	2.33	6.89E-01	71.70
	1.02E+06	*1.09E+07*	*0.39*	*3.76E-01*	*46.32*
13	3.34E+07	4.78E+07	4.78	3.09E+00	49.73
	1.31E+06	*2.94E+07*	*0.40*	*1.72E-01*	*76.04*
14	3.12E+05	2.59E+07	0.57	1.31E-01	53.39
15	7.40E+04	2.44E+07	0.63	5.78E+02	34.77
16	8.11E+07	3.07E+08	1.30	4.51E+08	51.30
	5.66E+06	*7.77E+07*	*0.44*	*7.18E+01*	*73.27*
	1.67E+05	*3.31E+06*	*0.49*	*7.79E+01*	*38.06*
17	3.02E+07	2.32E+08	1.05	3.71E+06	70.86
	1.86E+05	*2.10E+07*	*0.27*	*5.88E+00*	*69.99*
18	4.40E+05	4.54E+07	0.31	9.46E+00	76.05
19	2.46E+05	3.99E+07	0.38	3.02E+01	75.06
20	2.74E+05	7.94E+07	0.43	5.57E+01	68.15
21	1.43E+07	3.93E+07	1.58	2.37E+10	75.31
	1.59E+05	*1.43E+07*	*0.47*	*1.01E+02*	*66.53*
22	1.59E+07	4.95E+07	0.67	2.47E+03	48.91
	1.24E+05	*1.62E+07*	*0.34*	*1.47E+01*	*62.59*
23	1.02E+07	1.58E+08	0.45	6.72E+06	30.43
	4.21E+05	*6.50E+06*	*0.36*	*3.37E+00*	*40.27*
24	7.55E+05	3.65E+07	0.31	1.12E+01	50.34
25	2.86E+05	2.01E+07	0.26	3.48E+00	50.49
26	2.97E+06	1.01E+07	0.60	7.05E+02	58.36
	1.11E+06	*3.46E+06*	*-0.78*	*9.77E-07*	*46.32*
27	9.97E+05	3.13E+07	0.88	2.85E+04	30.47
	1.18E+05	*1.24E+06*	*-0.34*	*1.12E-03*	*28.06*
28	1.18E+06	1.83E+07	0.95	1.02E+05	46.05
29	2.30E+05	1.68E+07	0.55	2.79E+02	63.57
30	2.55E+06	1.62E+07	1.84	2.01E+11	83.75
31	2.18E+05	2.63E+06	0.10	5.53E-01	55.07
	4.49E+05	*1.79E+07*	*0.82*	*1.45E+04*	*59.15*
32	6.19E+04	1.64E+07	0.44	2.40E+01	27.27
33	1.26E+05	1.30E+07	0.71	1.47E+03	34.92
34	3.84E+06	3.03E+07	1.63	7.48E+09	43.13
	1.49E+05	*4.01E+06*	*0.59*	*2.53E+02*	*30.16*
35	1.10E+05	1.37E+07	0.70	1.02E+03	22.89
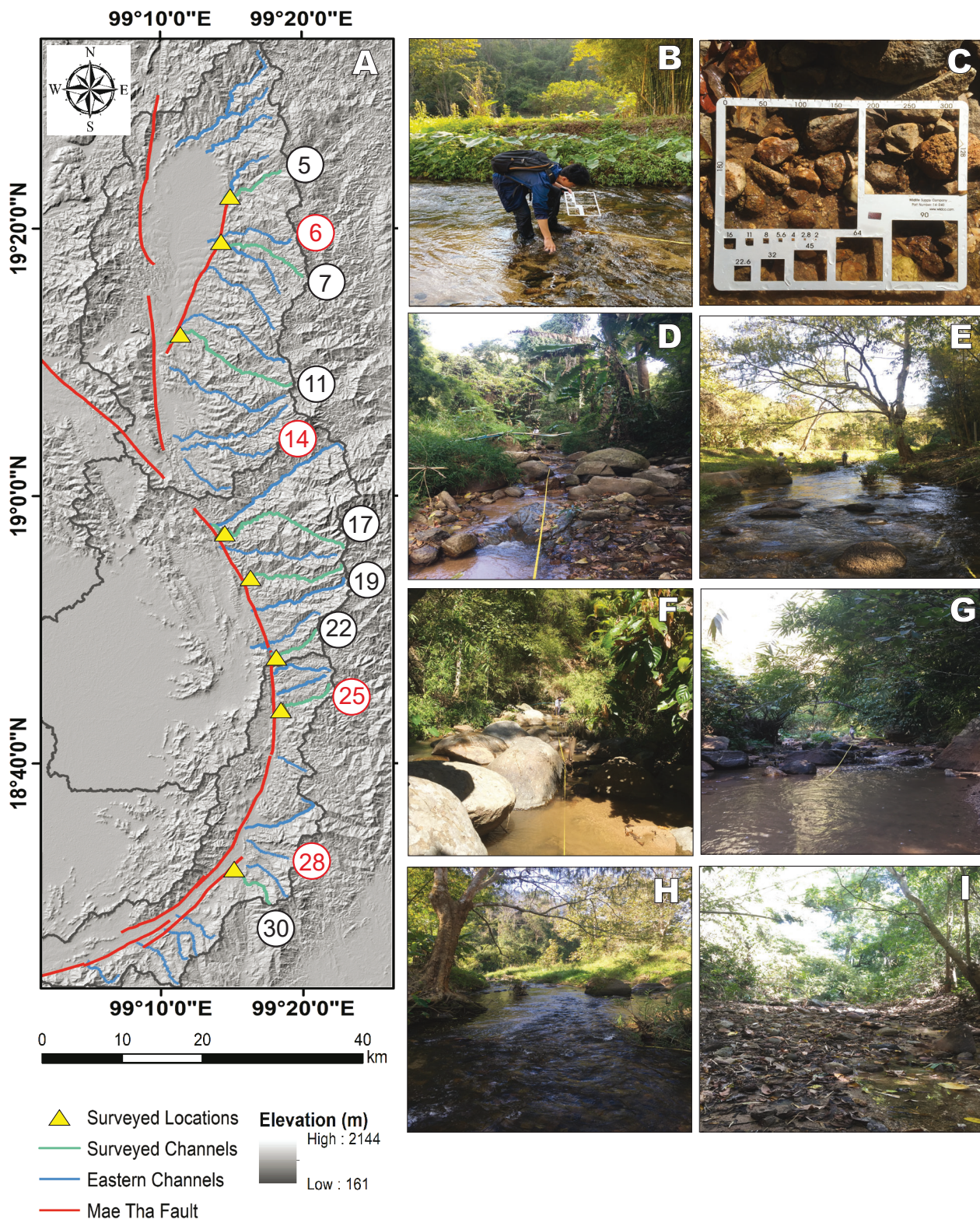
FIGURE 7. Field observations of lower-order channels along the eastern side of the MTF. A) Numbers in black circles represent the locations of our eight lower-order surveyed channels from north to south. The selection of channels is planned to survey across a range of channel steepness indices from north to south, including those channels with prominent knickpoints. The number in red circles exhibits channel profiles in Figure 8A-B. B-C) The method to measure bedload channels relies on the Wolman pebble count technique. C) An example of the measurement of bedload on channel bars and beds through the smallest hole that the grain can be fitted through. D-I) Examples of channel morphology surveys along channels 5, 7, 17, 19, 25 and 30, respectively. Channel bed is typically mantled with sub angular -sub rounded pebble to boulder clasts with the overall decrease in grain size toward the south. The photos were taken on channel beds during the winter season of February 2022.
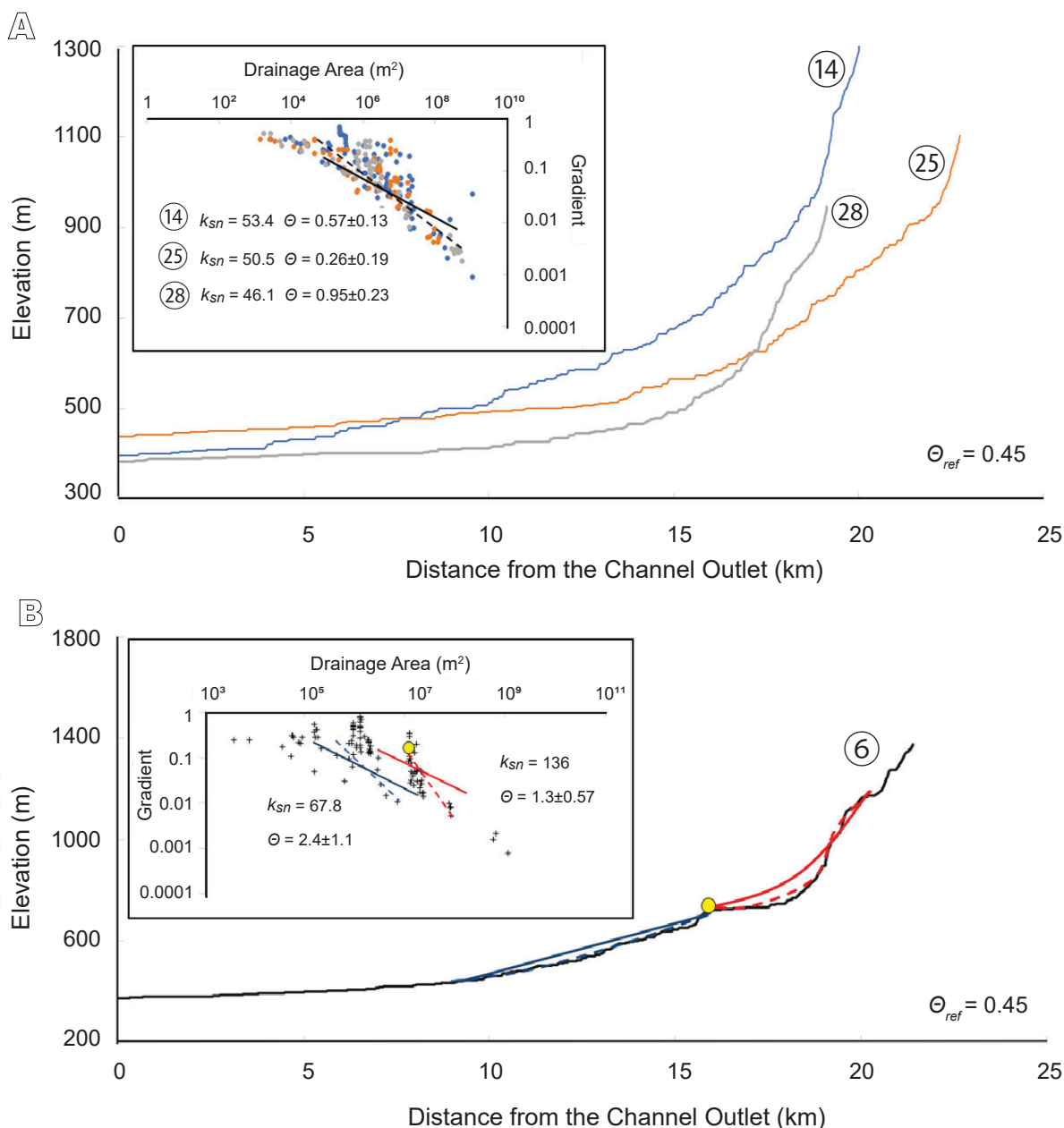
FIGURE 8. Representation of channel profiles along the eastern side of the MTF. A) Comparison of longitudinal channel profiles from channels 14, 25, and 28. The figure represents a concave-up channel profile with similar normalized channel steepness indices (k_{sn}) values. The dashed line in the inset shows an example of slope-area data for characterizing channel steepness (k_{sn}) and concavity (θ) of channel 25. The solid line regression with reference concavity (θ_{ref}= 0.45) is used to determine the normalized channel steepness indices (k_{sn}). B) An example of a longitudinal profile in a transient state channel (channel 6) that is characterized by a distinct convex knickpoint (marked by a yellow dot). The knickpoint separates the steeper upstream segment from the gentler downstream segment. The inset shows two different regressions of each segment above and below the knickpoint and provides differential k_{sn}.

characteristics of channel profiles along the eastern block of the MTF.

Collectively, k_{sn} values on channels are categorized into two data groups: the first group is k_{sn} of channel segments below the cluster of knickpoints; we found the overall slight decrease or constant k_{sn} values from north the south. We can fit a straight line to the wide scatter data of k_{sn} values with r^2= 0.23. The second group is k_{sn} in the upper channel reaches above the cluster of knickpoint; we found a threefold to fourfold decline in k_{sn} values from north to south. An exponential function best fits the data with r^2= 0.5 (Fig. 9B). Despite the wide scatter of the data, we consider that the range of threefold to fourfold decrease in k_{sn} values is
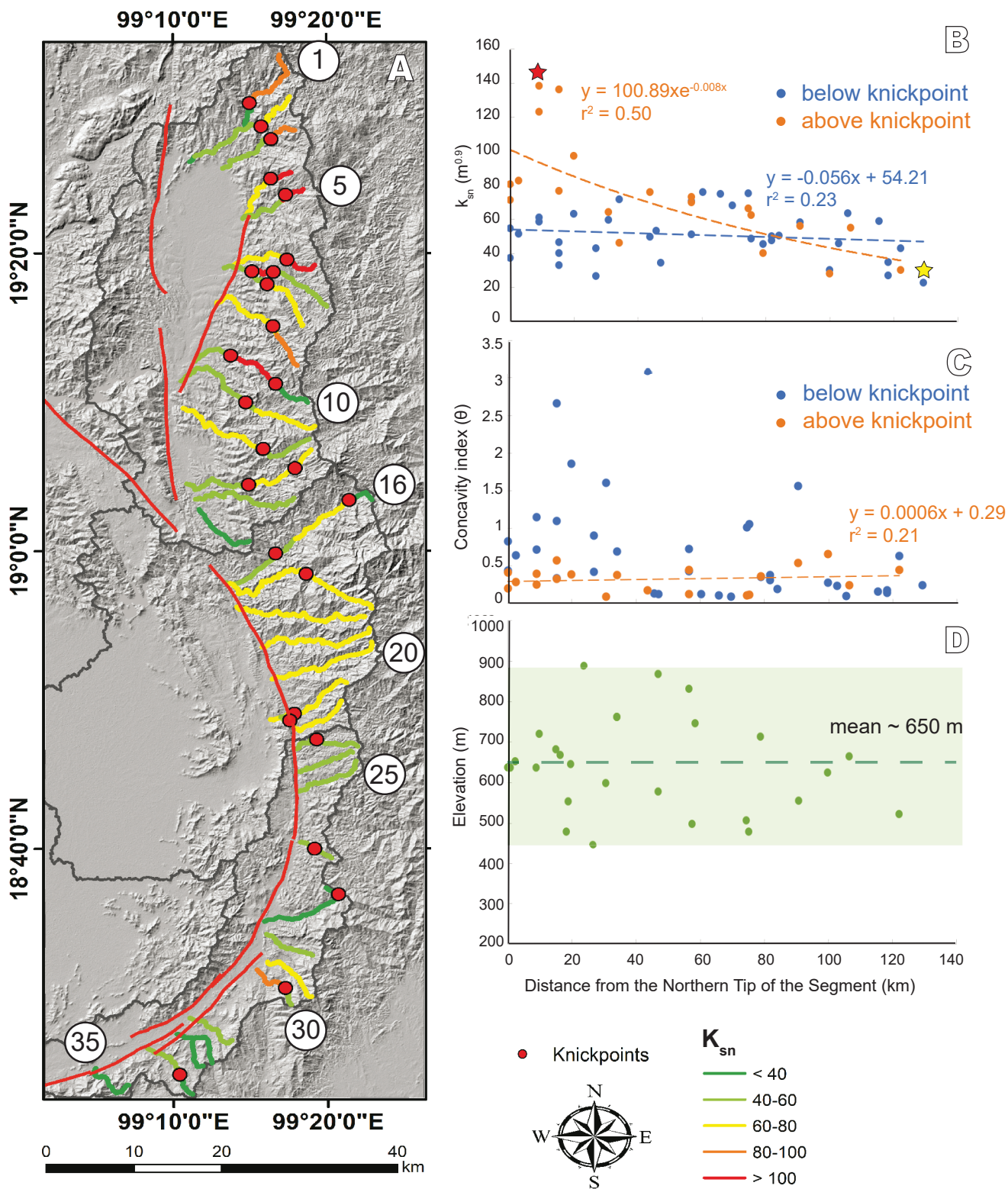
FIGURE 9. Topographic characteristics of channels along the eastern side of the MTF. A) Map of variations in normalized channel steepness indices (k_{sn}). Red dots represent knickpoints that mark the boundary between channel segments with different k_{sn}. B) Variations in normalized channel steepness indices (k_{sn}). Oranges dots represent normalized channel steepness indices on channel segments above knickpoints, while blues dots represent normalized channel steepness indices on channel segments below knickpoints. The red and yellow stars indicate the highest k_{sn} value at channel 4 and the lowest k_{sn} value at channel 35, respectively. C) Channel concavity (θ) as a function of distance from the northern tip of the segment. D) The elevation of knickpoints from north to south ranges between 450 and 900m with a regional mean of 650m.

reasonable with the degree of uncertainty in the data. For channel concavity indices (θ), the channel reaches above knickpoint display constant θ at ~0.3 with a low coefficient of the determinant ($r^2= 0.21$), despite the reduction of k_{sn} values from north to south (Fig. 9C).

The cluster of knickpoints found along longitudinal channel profiles is likely associated with spatial variations in k_{sn} and channel gradients, particularly a cluster of knickpoint in the northern zone. These channels typically exhibit steeper channel reaches above knickpoints than gentler downstream reaches. Channel segments above knickpoints exhibit the average k_{sn} at $>100m^{0.9}$, while the average k_{sn} below knickpoint is ~$60m^{0.9}$. The altitude of knickpoint ranges between 450 and 900m above sea level with a regional mean of 650m (Fig. 9D). The presence of knickpoint gradually disappears along channels toward the south.

Despite the low standard range of r^2 in these k_{sn} and θ values, the results primarily represent the spatial variations in normalized channel gradients and steepness. We used them to interpret the history of uplift and channel incision across the region.

Spatial variations in fracture density

The MTF is considered moderate-to-high seismic activities that are likely to produce different levels of fractures. A region close to the MTF may experience high levels of damage and generate a cluster of fractures relative to a distant region to the MTF. As a result, we characterize the different levels of fractures on the map (Fig. 10A). These features were verified by field observations and are described in the next section.

The detailed map of lineaments yields the spatial variation in fracture density across the landscape. We categorize the degree of fracture density into five different levels based on the statistically natural Jenks optimization method: none, low, moderate, high, and very high (Fig. 10B). Generally, the high level of fracture density distributes along the trace of the MTF. The values of fracture density decline toward the distant regions from the active major and minor faults. According to Figure 10B, the low level of fracture density distributes along the western side of the MTF. Along the eastern terrain of the MTF, the northern and central terrains experience a moderate fracture density, ranging from 0.96-1.5mkm^{-2}. The high level of fracture density appears along the Mae Kuang Fault (MKF) and continues to the southern zone. The southern tip of the study site exhibits a very high fracture density, approximately 1.5-4.4mkm^{-2} (Fig. 10B).

Geological field data and sediment analysis

Along the Thai National Highway 1150 in Phrao district, we found N-S striking fault planes dipping 40-70º

to the west (Fig. 6B-D). The evidence is well-preserved on the outcrops of the granite. In the central zone, the exposure of slicken lines and slickensides along Mae On and Mae Ruam rivers is plotted on the Faultkin® program. They are displayed on a stereonet and a rose diagram to infer the fault planes and their movement direction (Fig. 11A). These data can be separated in two major groups based on orientations of slickensides on fault surfaces and directions of the plunge of slicken lines:

• A first group of six fault planes illustrates ENE-WNW trending strike-slip faults with steep dipping (60-70º). The principal compressional stress comes from the northwest-to-west direction. Slicken lines plunge toward the west with variations in angles of plunge (Fig. 11B)

• A second group of six fault planes represents NNE-SSW oblique normal faults with steep dipping (60-80º). The principal extensional stress is along the east-west direction. Most slicken lines plunge toward the northeast-to-east directions with steep angles of plunge (Fig. 11C).

According to all lineaments, the combination of northwest compression and east-west tension suggests that the central segment of the MTF could be an extensional strike-slip duplex where the fault combines strike-and normal-slip fitting the model proposed by Woodcock and Fisher (1986).

The analysis of sediment bedload in eight channels reveals that overall sediment grain size varies from north to south across the eastern terrain of the MTF (Fig. 12). The group of median sediment particles ranges from granules to very coarse pebbles (>2-6cm) along channels in the northern and central zones. The largest median bedload is approximately 6cm on channel 19. Toward the south, there is a gradual decrease in the median sediment particle size to reach 2.7cm on channel 30 (Table 3; Fig. 12). Our results reveal that the median sediment bedload and its variance in the population (as described by the difference between D_{10} and D_{90}) vary relative to variations in k_{sn} values; higher k_{sn} values correlate with coarser bedload, while lower k_{sn} values correspond smaller sediment bedload size.

DISCUSSION

Implications of variations in geomorphic indices to rock uplift

The value of the channel steepness index is a proxy for rock uplift in steady-state mountain ranges (Kirby *et al.*, 2003, 2007; Kirby and Whipple, 2012; Snyder *et al.*, 2003), while channel concavity indices inversely vary with rock uplift (Hurst *et al.*, 2019). However, the normalized channel
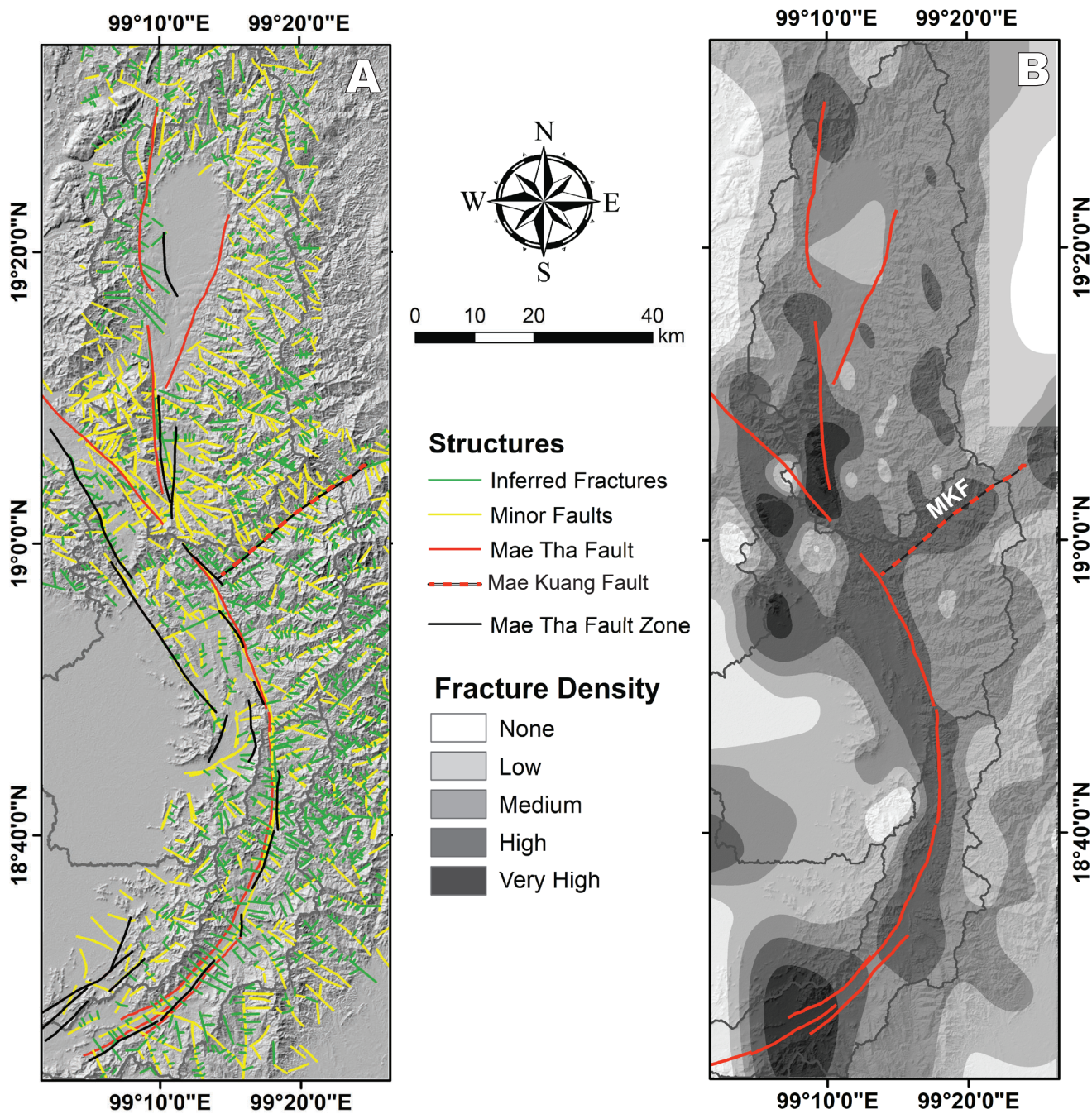
FIGURE 10. Topographic characteristics of channels along the eastern block of the MTF. A) Map illustrates lineaments that are classified into different categories. The MTFZ (black), MTF (red), MFK (red and black dashed) and minor faults (yellow) are defined by exposed lineaments on digital images, whereas fractures (green) are inferred from the rectangular drainage pattern. B) Map of distribution of fracture density (D). The highest fracture density is along the MTF, while the lowest fracture density is at distant areas from the main fault.

steepness index (k_{sn}) is more indicative of rock uplift, and it can be used to compare channels of different sizes (Kirby and Whipple, 2012).

Our topographic analysis shows a three-to-fourfold decrease in normalized channel steepness indices toward

the south, implying the decrease in rock uplift toward the south. Knickpoints /or slope breaks distributed in the middle segments of concave-up channel profiles suggest differences in rock uplift in upper and lower reaches; the upper reaches experience higher rock uplift relative to the lower reaches as described in other settings by Hurst
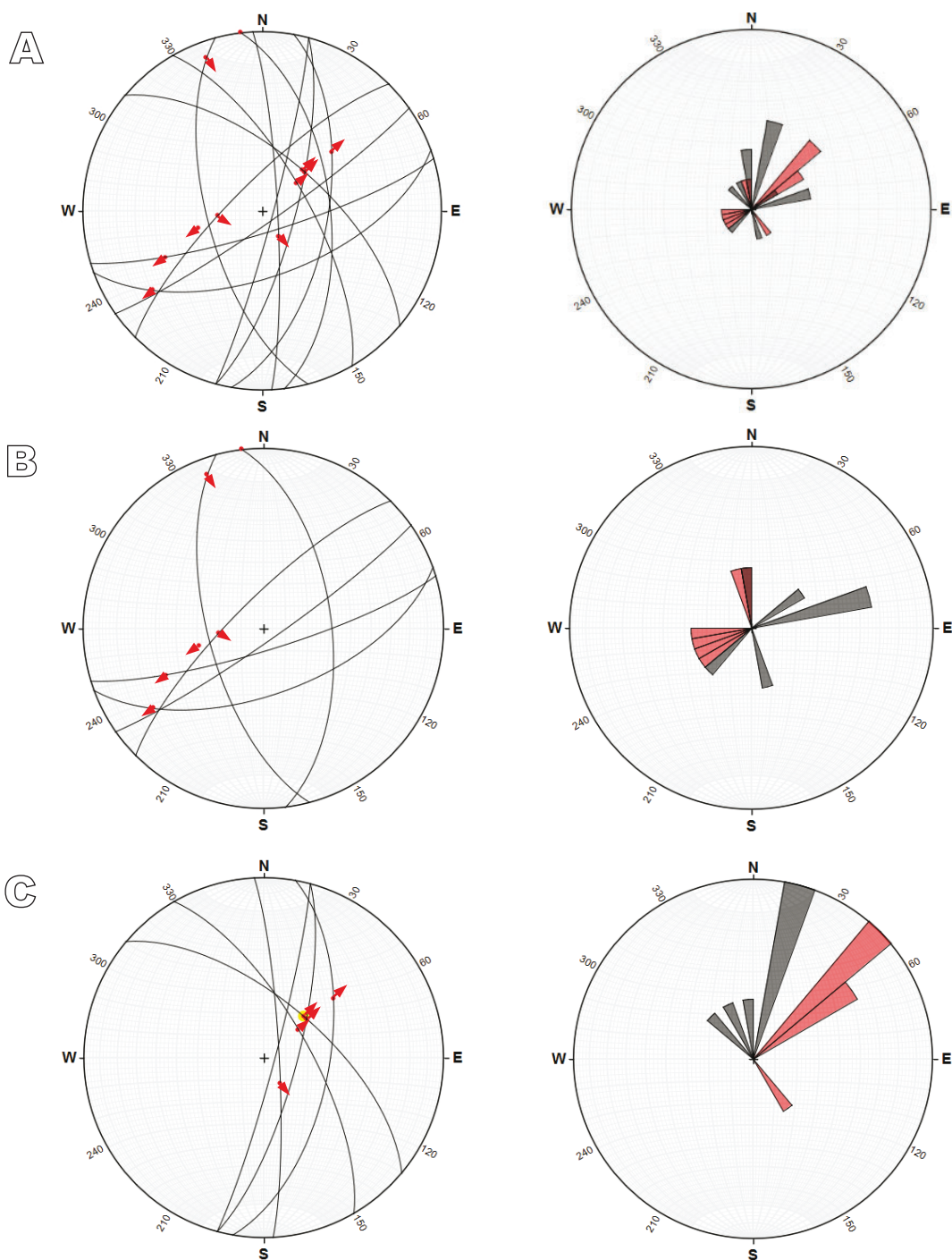
FIGURE 11. A) A collection of geologic structures that are recorded on rock surfaces along Mae On and Mae Ruam rivers. The left figure shows the slickenside of fault planes (black line) and slicken lines (red dots with arrows) plotted on a stereonet. The right figure shows the slickenside of fault planes (black polygons) and slicken lines (red polygon) plotted on a rose diagram. B) A group of slickensides orients in the ENE-WNW direction with slicken lines toward the west. C) A group of slickensides orients in the NNE-SSW direction with slicken lines toward the east.

et al. (2019), and Wickert and Schildgen (2019). Such a landscape is confirmed to be in a transient state condition where channels respond to the temporal variation in rock uplift. Since the MTF has no strong variations in climatic gradients, the variation in channel morphology is not likely dominated by different climatic conditions. Variations

in tectonic and lithologic forcing drive the landscape adjustment across the MTF.

The simple bedrock incision model can describe channel adjustment along the eastern terrain of the MTF. The mechanistic basis of stream power (the effect of the

TABLE 3. The average grain size along each channel and their distribution

Channel number	D_{10} (mm)	D_{50} (mm)	D_{90} (mm)
5	23	55	88
7	9	23	49
11	14	33	65
17	18	34	61
19	24	58	88
22	17	35	110
25	18	40	96
30	11	27	62

combination of discharge and channel gradient) leads to channel incision rate increase and channel steepening as rock uplift increases. However, the exponential decrease in channel steepness in the upper channel reaches is governed by variations in sediment grain size (Fig. 9B). This pattern suggests that a simple bedrock incision is unrealistic to describe the bedrock channel incision during regular events. Sediment particle size is likely to be an influential factor in controlling bedrock channel incisions (*e.g.* DiBiase and Whipple, 2011; Sklar and Dietrich, 1998).

We interpret the pattern of rock uplift across the eastern terrain of the MTF as reflecting a process where i) channels adjust their morphology to the spatial variation in rock uplift rates associated with resistant rock, surficial processes on the landscape, and the fault movement and ii) the entire landscape is in the transient-state condition, adjusting to differential rock uplift rates. The pattern can be observed from the variation in the elevation of knickpoints that knickpoints underlain by granitic and granodioritic rocks with moderate fracture density are in relatively high elevations. In contrast, knickpoints in lower elevations are located in the clastic sedimentary rocks with higher fracture density. Our analysis averages the mean elevation of knickpoints at 650m above sea level. Channels adjust their morphology and appear to retreat at the same rate controlled by the changes in rock uplift.

Channel steepness as a function of lithologic forcing

The eastern side of the MTF is a topographically rugged terrain in the mixed deciduous forest. The terrain is composed of the Triassic Doi Saket-Wiang Pa Pao granitic batholith intrusion into the Paleozoic clastic-to-metamorphosed sedimentary rocks (Nakapadungrat *et al.*, 1984). Variable rock types could play a significant role in controlling spatial variation in channel adjustment.

The large extent of granite on the eastern terrain can be seen from aerial/satellite images and field observations.

The resistance of homogeneous granite is typically higher than clastic sedimentary rocks for weathering processes. Thus, channels exhibit different channel profiles and steepness: channel steepness in the upper reaches is twice to threefold higher than that in the lower reaches (Table 2; Fig. 9B). The differences in channel steepness imply that erosional processes on the granitic terrains are slower than the terrain underlaid by older clastic and meta clastic-sedimentary rocks (Fig. 13A).

Although less-resistant clastic and metamorphic rocks underlie the downstream segments of channels in the northern zone, the presence of steeper lower channel reaches results from the coverage of large granitic pebbles and cobbles that are eroded and delivered from the steeper upper channel reaches. The cover effects from large sediment particles on the channel bed control the Channel incision (Sklar and Dietrich, 1998; 2006). These channel segments may be transferred to a transport-limited state where the high volume of sediment supply and larger size of sediment materials limits channel incision and channel steepness. Channel incision can re-occur when high shear stress/or stream power exceeds the threshold shear stress from the cover effect (Snyder *et al.*, 2003; Stock and Montgomery, 1999; Tucker, 2004). The influences of cover effects and rock resistance may potentially make channels steeper along the eastern block of the MTF.

Although the granitic lithologies underlie channels in the southern section, these present shorter and gentler channel profiles with lower channel steepness values. The sediment particle sizes on the channel bed are smaller compared to channels in the northern zone. The smaller
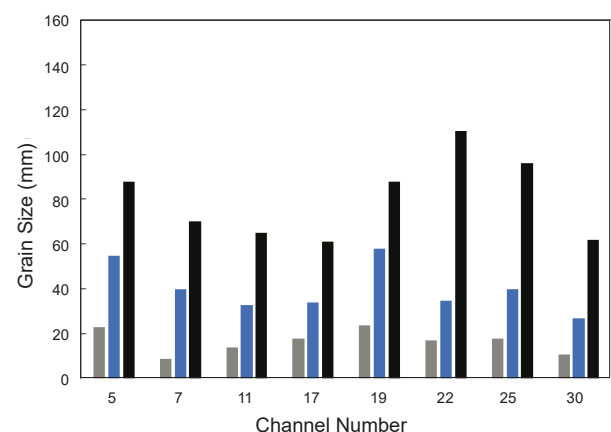

FIGURE 12. Determination of grain size distribution on eight surveyed channels along the eastern block of the MTF. The locations of channels are shown in Figure 9A. The result of averaged grain size distribution illustrates that the median bedload sizes are large in channels 5 and 19. However, the median particle sizes become smaller toward the South. The figure represents variations in the relationship between channel steepness and their variance in the population (as described by the difference between D_{10} and D_{90}). Grey: D_{10} (mm), Blue: D_{50} (mm), Black: D_{90} (mm).
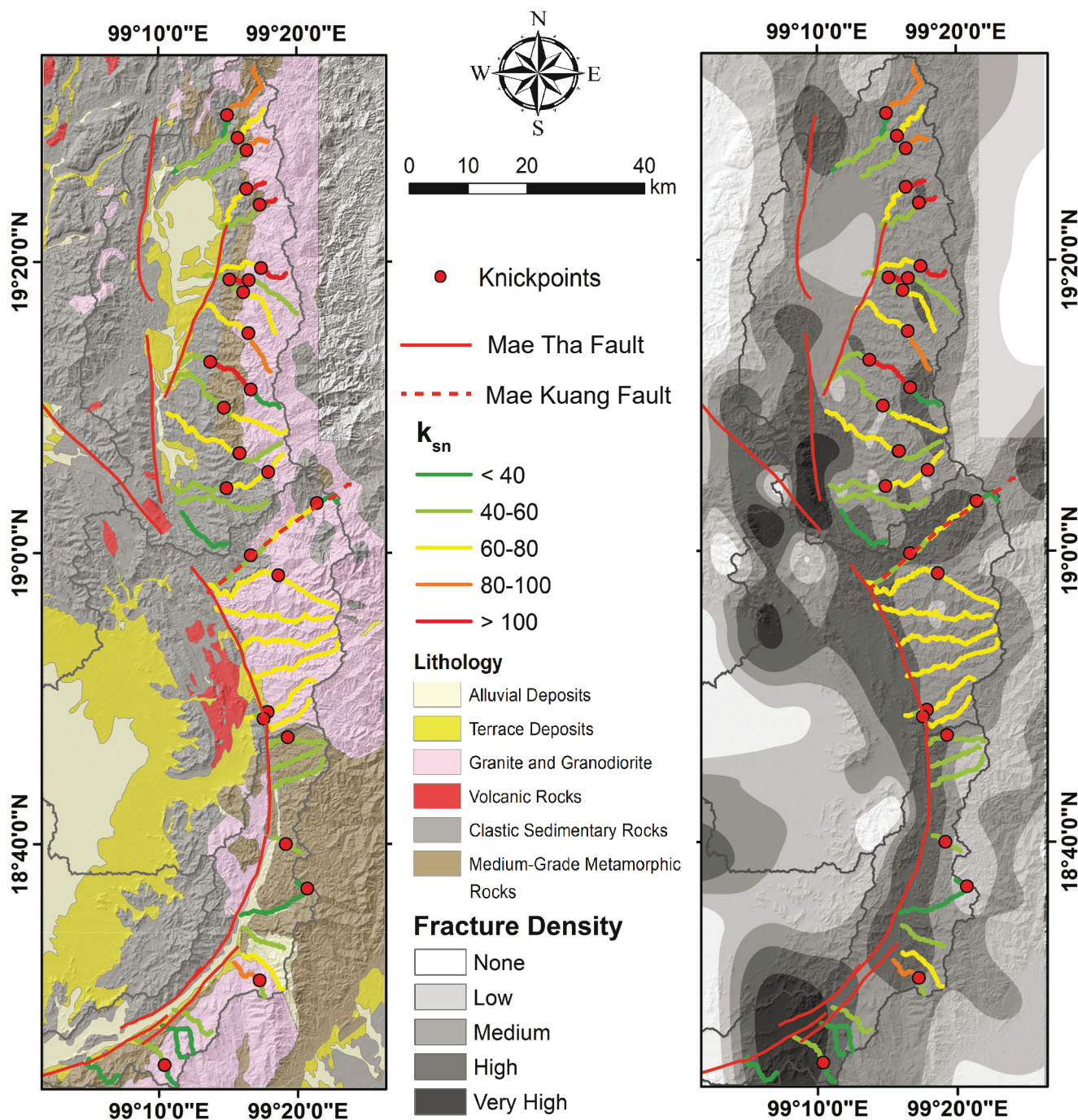
FIGURE 13. A) The relationship between channel steepness indices and the distribution of rock units along the eastern side of the MTF. In the northern zone, the steeper upstream channel reaches are strongly related to the granitic intrusion, whereas more downstream channel reaches are underneath by older clastic sedimentary rocks. The resistant granitic intrusion plays a significant role in making the channel steeper in the central zone. However, channels in the southern zone decrease their steepness values because granitic intrusion and medium-grade metamorphic bedrock underlie them. Red dots indicate the positions of knickpoint that are typically located near the boundary between granitic intrusion and sedimentary rocks. B) The relationship between channel steepness indices and fracture density distribution along the eastern side of the MTF. High values of channel steepness in the northern and central zones correspond to the medium level of fracture density. However, low values of channel steepness in the south are underneath by rocks with a high-to-very high level of fracture density, particularly along the southern tip of The segment. Knickpoints distribute in locations of a moderate level of fracture density.

particle size on the channel bed weakens the cover effect, allowing for a faster rate of fluvial erosion on the channel bed. Due to the spatial changes in channels and topography, tectonic processes are likely to be an essential factor driving the different behavior of channel characteristics in the south.

Channel steepness as a function of tectonic forcing

In a transient-state fluvial system, channels adjust their morphology to tectonic uplift and have not yet attained a steady-state condition. The channel steepness, channel width, and sediment cover patterns on the channel bed are spatially variable. Although we did not observe the change in channel width in field observations, the channel width is variable throughout the length of the channels. Our analysis is restricted to the adjustment of channel profiles as the preliminary sign of landscape adjustment to tectonic and lithologic forcing. Previously, we realized that the northern channel profiles, and channel steepness are controlled by lithologic strength and the cover effects from larger sediment particles. Tectonically, the northern section is bounded by a west-dipping normal fault. The relative movement of the footwall side (a terrain underlaid by granite and Paleozoic clastic sedimentary rocks) rises the terrain's elevation, which makes upstream channels steeper, and higher rock uplift.

In the central zone where terrain and topographic gradients are still high, the coupled effects of lithologic resistance and the cover effects make channels steeper. The movement of the sinistral-lateral strike slip MKF with respect to the MTF causes a differential motion and uplift between adjacent rotating blocks (Rhodes *et al.*, 2004). The tectonic uplift exposes the wall rocks to the east and west of granitic batholith consisting of interbedded white quartz-rich sandstone and shale of the Carboniferous Mae Tha Formation. (Uttamo, 2000). The uplift steepens channels on resistant granitic bedrock. The evidence of an extensional strike-slip duplex exposed along Mae On and Mae Ruam rivers seems to explain the landmass's exhumation to a higher elevation.

The altitude of topography in the south is lower than that in the northern and central zones. The influences of lithologic substrates and cover effects may be subordinate to the role of tectonics and lineaments in controlling the shape of the terrain and the adjustment of channels. Due to the lower presence of local lineaments, the fault-related geomorphic features help to infer an oblique-slip fault of the southern segment of the MTF. A reasonable explanation to lower elevation and gentler channel steepness in the southern zone is that these features are controlled by the high to very high density of fracture (Fig. 13B). The interconnection between the major MTF, minor faults, and

inferred fractures makes this zone highly fractured and highly susceptible to weathering and erosion rate. Rock mass strength decreases, leading to smaller sediment grain size transported to channel networks. The weaker cover effects from smaller clasts cannot protect the channel bed from fluvial erosion. Thus, the height of the topographic landmass is reduced (Molnar *et al.*, 2007; Roy *et al.*, 2016).

When comparing the spatial distribution of fracture density across the eastern terrain of the MTF, fracture density is inversely proportional to channel steepness and channel gradient; the moderate level of fracture density in the northern and central zones correlates to higher channel steepness and gradients, while the higher level of fracture density in the south associates with gentler channels and lower terrains. Therefore, the connection between tectonic processes, fracturing, and rock erodibility of the landscape influences lower landscape topography all along the region.

This study shows the roles of tectonic and lithologic factors in controlling landscape topography along the MTF. At the same time, it serves as an example of how geomorphic analysis helps to understand landscape adjustment and evolution in tectonically active regions with similar conditions.

CONCLUSION

Longitudinal channel profiles and channel steepness indices help to characterize the spatial adjustment of terrain morphology due to rock uplift. Our study focuses on the adjustment of channels to the influence of tectonic and lithologic forcing along the eastern terrain of the Mae Tha fault, in which variable rock mass quality and lineaments are present. Our topographic analysis reveals a three-to-fourfold decrease in channel steepness indices from north to south, implying the overall decrease in rock uplift. At sites where knickpoints are present, the upper reaches of the channel are steeper than the lower reaches.

The differential decrease in rock uplift across the region correlates to less-resistant geologic substrates, smaller sediment particles delivered to channel networks, and spatial changes in linear structures. In the northern and central zones, steeper channels and high terrains are controlled by resistant homogenous granitic rocks on the footwall side of the terrain and the strong cover effects of coarse bedload on the channel bed. Conversely, gentler channels and lower terrains in the south are controlled by an oblique-slip fault and a high fracture density. Our study confirms that the roles of lineaments, rock mass quality, and sediment particles can control spatial adjustment of landscape topography across the eastern block of the Mae Tha fault. Overall, our study provides an insight that the

use of topographic adjustment analysis may contribute to explain the dynamics of active deformation of the landscape over space and time and to evaluate tectonic and lithologic forcing in tectonically active mountain ranges.

ACKNOWLEDGMENTS

REFERENCES

Burbank, D.W., Anderson, R.S., 2012. Tectonic Geomorphology. United Kingdom, Blackwell Publishing, 454pp.

Charusiri, P., Clark, A.H., Farrar, E., Archibald, D., Charusiri, B., 1993. Granit belts in Thailand: evidence from the 40Ar/39Ar geochronological and geological syntheses. Journal of Southeast Earth Sciences, 9(1-4), 127-136.

Department of Mineral Resources, 2008. The study of recurrent intervals from fault movement in Chiang Mai, Lamphun, Lampang, and Phrae (Mae Tha and Thoen faults). Bangkok, Department of geology, Faculty of Science, Chulalongkorn University, 392pp.

Department of Mineral Resources, 2018. Earthquakes and Thailand. Bangkok, Environmental Geology Division, Department of Mineral Resources, 53pp.

Department of Mineral Resources, 2020. Atlas book of maps of active faults in Thailand. Department of Mineral Resources, Bangkok, 32 pp.

DiBiase, R.A., Whipple, K.X., 2011. The influence of erosion thresholds and runoff variability on the relationships among topography, climate, and erosion rate. Journal of Geophysical Research, 116, F04036. DOI: 10.1029/2011JF002095

DiBiase, R.A., Whipple, K.X., Lamb, M., Heimsath, A., 2015. The role of waterfalls and knickzones in controlling the style and pace of landscape adjustment in the western San Gabriel Mountains, California. Geological Society of America Bulletin, 127(3-4), 539-559. DOI: 10.1130/B31113.1

Dietrich, W.E., Bellugi, D.G., Sklar, L.S., Stock, J.D., Heimsath, A.M., Roering, J.J., 2003. Geomorphic transport law for predicting landscape form and dynamics. Prediction in Geomorphology, Geophysical Monograph Series, 135, 103-132.

Duvall, A., Kirby, E., Burbank, D., 2004. Tectonic and lithologic controls on bedrock channel profiles and processes in coastal California. Journal of Geophysical Research, 109, F03002. DOI: 10.1029/2003JF000086

Flint, J.J., 1974. Stream gradient as a function of order, magnitude, and discharge. Water Resources Research, 10(5), 969-973.

Hilley, G., Porder, S., Aron, F., Baden, C., Johnstone, S., Liu, F., Sar, R., Steelquist, A., Young, H.H., 2019. Earth's topographic relief potentially limited by an upper bound on channel steepness. Nature Geoscience, 12(10), 828-832.

Howard, A.D., 1967. Drainage analysis in geologic interpretation: A summation. American Association of Petroleum Geologists (AAPG) Bulletin, 51, 2246-2259.

Howard. A.D., Dietrich, W., Seidl, M., 1994. Modeling fluvial erosion on regional to continental scales. Journal of Geophysical Research: Solid Earth, 99(B7), 13971-13986. DOI: 10.1029/94JB00744

Hurst, M.D., Mudd, S., Walcott, R., Attal, M., Yoo, K., 2012. Using hilltop curvature to derive the spatial distribution of erosion rates. Journal of Geophysical Research: Earth Surface, 117, F02017. DOI: 10.1029/2011JF002057

Hurst, M.D., Grieve, S.W.D., Clubb, F.J., Mudd, S.M., 2019. Detection of channel-hillslope coupling along a tectonic gradient. Earth and Planetary Science Letters, 522, 30-39. DOI: 10.1016/j.epsl.2019.06.018

Khamkong, M., Bookkamana, P., Shin, Y., Park, J.S., 2017. Modelling extreme rainfall in Northern Thailand with estimated missing values. Chiang Mai Journal of Science, 44(4), 1792-1804.

Kirby, E., Whipple, K., 2001. Quantifying differential rock-uplift rates via stream profile analysis. Geology, 29(5), 415-418.

Kirby, E., Whipple, K., Tang, W., Chen, Z., 2003. Distribution of active rock uplift along the eastern margin of the Tibetan Plateau: Inferences from bedrock channel longitudinal profiles. Journal of Geophysical Research: Solid Earth, 108(B4), 2217. DOI: 10.1029/2001JB000861

Kirby, E., Johnson, C., Furlong, K., Heimsath, A., 2007. Transient channel incision along Bolinas Ridge, California: Evidence for differential rock uplift adjacent to the San Andreas fault. Journal of Geophysical Research, 112, F03S07. DOI: 10.1029/2006JF000559

Kirby, E., Whipple, K., 2012. Expression of active tectonics in erosional landscapes. Journal of Structural Geology, 44, 54-75. DOI: 10.1016/j.jsg.2012.07.009

Lague, D., Hovius, N., Davy, P., 2005. Discharge, discharge variability, and the bedrock channel profile. Journal of Geophysical Research: Earth Surface, 110, Fo4006. DOI: 10.1029/2004JF000259

Laurencelle, J., Logan, T., Gens, R., 2015. ASF radiometrically terrain corrected ALOS PALSAR products. Last accessed: January 2022. Website: https://asf.alaska.edu/wp-content/uploads/2019/03/rtc_product _guide_v1.2.pdf

Liu, J.G., Mason, P.J., Yu, E., Wu, M-C, Tang, C., Huang, R., Liu, H., 2012. GIS modelling of earthquake damage zones using satellite remote sensing and DEM Data. Geomorphology, 139-140, 518-535. DOI: 10.1016/j.geomorph.2011.12.002

Mankhemthong, N., Morley, C.K., Srichan, W., 2020. Structure of the Mae on depression, Chiang Mai Province, based on Gravity Modelling and geological field observation: Implications for tectonic evolution of the Chiang Mai -Chiang Rai Suture Zone, northern Thailand. Journal of Asian Earth Sciences, 190, 104186. DOI: 10.1016/j.jseaes.2019.104186

Mejia, A.I., Niemann, J.D., 2008. Identification and characterization of dendritic, parallel, pinnate, rectangular, and trellis networks based on deviations from planform self-similarity. Journal of Geophysical Research, 113, F02015. DOI: 10.1029/2007JF000781

Molnar, P., Anderson, R.S., Anderson, S.P., 2007. Tectonics, fracturing of rock, and erosion. Journal of Geophysical Research, 112, F03014. DOI: 10.1029/2005JF000433

Nakapadungrat, S., Beckinsale, R.D., Suensilpong, S., 1984. Geochronology and geology of Thai granites. In: Piancharoen, C. (ed.). Conference on Applications of Geology and the National Development. Bangkok, Chulalongkorn University, 75-93.

Pailoplee, S., Charusiri, P., 2016. Seismic hazards in Thailand: a compilation and updated probabilistic analysis. Earth, Planets and Space, 68(98), 1-14. DOI: 10.1186/s40623-016-0465-6

Pérez-Peña, J.V., Azanon, J.M., Booth-Rea, G., Azor, A., Delgado, J., 2009. Differentiating geology and tectonics using a spatial autocorrelation technique for the hypsometric integrals. Journal of Geophysical Research, 114, F02018. DOI: 10.1029/2008JF001092

Rhodes, B., Perez, R., Lamjuan, A., Kosuwan, S., 2004. Kinematics and tectonic implications of the Mae Kuang Fault, Northern Thailand. Journal of Asian Earth Sciences, 24(1), 79-89. DOI: 10.1016/j.jseaes.2003.09.008

Roy, S.G., Tucker, G.E., Koons, P.O., Smith, S.M., Upton, P., 2016. A fault runs through it: Modeling the influence of rock strength and grainsize distribution in a fault-damaged landscape. Journal of Geophysical Research: Earth Surface, 121, 1911-1930. DOI: 10.1002 /2015JF003662

Schmidt, K., Montgomery, D., 1995. Limits to Relief. Science, 270(5236), 617-620.

Sklar, L.S., Dietrich, W.E., 1998. River longitudinal profiles and bedrock incision models: Stream power and the influence of sediment supply. American geophysical Union Monograph, 107, 237-260. DOI: 10.1029/GM107p0237

Sklar, L.S., Dietrich, W.E., 2006. The role of sediment in controlling steady-state bedrock channel slope: Implications of the saltation-abrasion incision model. Geomorphology, 82, 58-83. DOI: 10.1016/j.geomorph.2005.08.019

Snyder, N.P., Whipple, K.X., Tucker, G.E., Merritts, D.J., 2000. Landscape response to tectonic forcing: Digital Elevation Model Analysis of stream profiles in the Mendocino triple junction region, Northern California. Geological Society of America Bulletin, 112(8), 1250-1263.

Snyder, N.P., Whipple, K.X., Tucker, G.E., Merritts, D.J., 2003. Importance of a stochastic distribution of floods and erosion thresholds in the bedrock river incision problem. Journal of Geophysical Research: Solid Earth., 108(B2), 2117. DOI: 10.1029/2001JB001655

Stock, J.D., Montgomery, D.R., 1999. Geologic constraints on bedrock river incision using the stream power law. Journal of Geophysical Research: Solid Earth, 104(B3), 4983-4993. DOI: 10.1029/98JB02139

Stock, J.D., Dietrich, W.E., 2003. Valley incision by debris flows: Evidence of a topographic signature. Water Resources Research, 39(4), 1089. DOI: 10.1029/2001WR001057

Tucker, G., 2004. Drainage basin sensitivity to tectonic and climatic forcing: implications of a stochastic model for the role of entrainment and erosion thresholds. Earth Surface Processes and Landforms, 29(2), 185-205. DOI: 10.1002/esp.1020

Uttamo, W., 2000. Structure and sedimentological evolution of the Tertiary sedimentary basins in northern Thailand. PhD dissertation Thesis. London (United Kingdom), University of London, 501pp.

Whipple, K.X, Tucker, G., 1999. Dynamics of the stream-power river incision model: Implications for height limits of mountain ranges, landscape response timescales, and research needs. Journal of Geophysical Research: Solid Earth, 104(B8), 17661-17674. DOI: 10.1029/1999JB900120

Whipple, K.X., Hancock, G.S., Anderson, R.S., 2000. River incision into bedrock: Mechanics and relative efficacy of plucking, abrasion, and cavitation. Geological Society of America Bulletin, 112(3), 490-503.

Whipple, K.X., Wobus, C., Crosby, B., Kirby, E., Sheehan, D., 2007. New tools for quantitative geomorphology: extraction and interpretation of stream profiles from digital topographic data. GSA annual meeting, 1-26.

Whipple, K.X., 2009. The influence of climate on the tectonic evolution of mountain belts. Nature Geoscience, 2(2), 97-104.

Whittaker, A., Attal, M., Cowie, P., Tucker, G., Roberts, G., 2008. Decoding temporal and spatial patterns of fault uplift using transient river long profiles. Geomorphology, 100(3-4), 506-526. DOI: 10.1016/j.geomorph.2008.01.018

Wickert, A.D., Schildgen, T.F., 2019. Long-profile evolution of transport-limited gravel-bed rivers. Earth Surface Dynamics, 7(1), 17-43. DOI: 10.5194/esurf-7-17-2019

Wiwegwin, W., Hinsaeng, P., Junpangngern, J., Phumsonklin, R., 2018. Characteristics of 15 active fault zones in Thailand. Bangkok, Department of Mineral Resources, 233pp.

Wobus, C., Crosby, B., Whipple, K., 2006. Hanging valleys in fluvial systems: Controls on occurrence and implications for landscape evolution. Journal of Geophysical Research, 111, F02017. DOI: 10.1029/2005JF000406

Woodcock, N.H., Fischer, M., 1986. Strike-slip duplexes. Journal of Structural Geology, 8(7), 725-735.

Yanites, B.J., Tucker, G.E., 2010. Controls and limits on Bedrock Channel Geometry. Journal of Geophysical Research, 115, F04019. DOI: 10.1029/2009JF001601